Journal of Colloid and Interface Science 705 (2026) 139493

Contents lists available at ScienceDirect

Journal of Colloid And Interface Science

journal homepage: www.elsevier.com/locate/jcis

Design and characterization of antibiotic-free lyotropic liquid crystalline coatings based on binary docosahexaenoic acid monoglyceride/glycerol monooleate systems for combating orthopedic implant-associated infections

Seref Akay [a,b,**], Oana Ciofu [c], Jonathan Michael Gow [d], Dorthe Posselt [d], Benedetta Marmiroli [e], Barbara Sartori [e], Anan Yaghmur [a,*]

[a] Department of Pharmacy, Faculty of Health and Medical Sciences, University of Copenhagen, 2200 Copenhagen, Denmark
[b] Department of Genetics and Bioengineering, Faculty of Engineering, Alanya Alaaddin Keykubat University, 07425 Alanya, Antalya, Turkey
[c] Department of Immunology and Microbiology, Costerton Biofilm Center, Faculty of Health and Medical Sciences, University of Copenhagen, 2200 Copenhagen, Denmark
[d] IMFUFA, Department of Science and Environment, Roskilde University, 4000 Roskilde, Denmark
[e] Institute of Inorganic Chemistry, Graz University of Technology, 8010 Graz, Austria

GRAPHICAL ABSTRACT

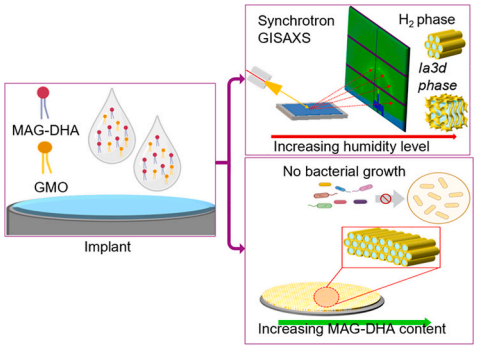

Abbreviations: BA, Born approximation; CFU, Colony forming unit; DI, Deionized water; DHA, Docosahexaenoic acid; DWBA, Distorted wave born approximation; EPA, Eicosapentaenoic acid; GISAXS, Grazing incidence small-angle X-ray scattering; HS-QCM-D, Humidity scanning quartz crystal microbalance with dissipation; GMO, Glycerol monooleate; LB, Luria-Bertani broth; LLC, Non-lamellar lyotropic liquid crystalline; MAG-DHA, Docosahexaenoic acid monoacylglycerol; MAG-DPA, Docosapentaenoic acid monoacylglycerol; MAG-EPA, Eicosapentaenoic acid monoacylglycerol; MIC, Minimum inhibitory concentration; Ω-3 PFAs, Omega-3 poly-unsaturated fatty acids; PIA, Polysaccharide intercellular adhesins; PGs, Phosphatidylglycerols; RT, Room temperature; SAXS, Small angle X-ray scattering; SS, Stainless steel; RH, Relative humidity; TSB, Tryptic soy broth..

* Corresponding author at: Department of Pharmacy, Faculty of Health and Medical Sciences, University of Copenhagen, 2200 Copenhagen, Denmark.
** Corresponding author at: Department of Genetics and Bioengineering, Faculty of Engineering, Alanya Alaaddin Keykubat University, 07425 Alanya, Antalya, Turkey.
E-mail addresses: seref.akay@alanya.edu.tr (S. Akay), anan.yaghmur@sund.ku.dk (A. Yaghmur).

https://doi.org/10.1016/j.jcis.2025.139493
Received 10 September 2025; Received in revised form 30 October 2025; Accepted 15 November 2025
Available online 17 November 2025

ARTICLE INFO

Keywords:
Antibacterial coatings
Biofilms
Docosahexaenoic acid monoglyceride
GISAXS
Inverse bicontinuous cubic phase
Inverse hexagonal phase
Orthopedic implants

ABSTRACT

There is a growing interest in innovative strategies for effectively preventing implant-associated bacterial infections. Here, we report on a simple-by-design approach for production of antibacterial coatings from docosahexaenoic acid monoacylglycerol (MAG-DHA) and glycerol monooleate (GMO). In addition to its amphiphilic nature, MAG-DHA is a safe precursor of docosahexaenoic acid (DHA) and has different beneficial health effects, including antibacterial activities. Using binary combinations of MAG-DHA and GMO, we describe the structural features and the antibacterial activities of antibiotic-free non-lamellar liquid crystalline (LLC) coatings. Small-angle X-ray scattering (SAXS) and *in situ* grazing incidence small-angle X-ray scattering (GISAXS) were employed to gain insight into the structural features of the fully hydrated coatings and the hydration-induced dynamic self-assembly of MAG-DHA and GMO on model implants. In a lipid composition-dependent manner, SAXS results revealed hydration-induced formation of different inverse LLC self-assemblies, including hexagonal (H_2) and bicontinuous cubic (Q_2) phases. Further, GISAXS analysis showed that lipid composition and employed relative humidity level play important roles in controlling the out-of-equilibrium self-assembly properties. Moreover, the coatings containing MAG-DHA displayed unique inherent antibacterial activities against *Staphylococcus aureus* and *Staphylococcus epidermidis* strains. This study describes the first antibiotic-free coatings with nanostructural architectures and inherent antibacterial activities for orthopedic implants.

1. Introduction

There is a rapid growth worldwide in the number of implantable devices (> 500,000), including prosthetics, catheters, and scaffolds. Therefore, it is becoming increasingly important for the orthopedic community to introduce safe and efficacious strategies for combating biofilm infections, which represent a major public health burden [1–3]. Among these devices, natural and synthetic orthopedic implants are attractive for improving the patient life quality through simulating regeneration of tissues and re-establishment of their functions [4,5]. However, surgical implantation procedures are typically associated with development of persistent bacterial implant infections, which can spread to adjacent tissues [6]. Further, such infections may lead to extended treatment periods, increased morbidity among hospitalized patients, and even implant failure [7–11].

Biofilms are dense 3D matrices built of polysaccharides, fibrous proteins, and lipoproteins. They prevent penetration of antibiotics to the encased bacteria and inhibit the immune responses [12,13]. It is, therefore, challenging to treat biofilm infections. Over the past few decades, about 50% of reported failures have been ascribed to poor integration of orthopedic implants with the surrounding tissues and development of biofilm infections [14]. These infections account for 25% of clinical infections (including about 0.8–2% of infections associated with prosthetic replacement surgeries) [15]. Further, within five years of post-surgery complications, the caused mortality rate can reach up to 21%, which is comparable to the reported mortality rates for breast cancer and melanoma [2,11,15]. Systemic antibiotic treatments and revision surgeries are considered gold standards for treating and preventing biofilm infections [15,16]. Nonetheless, systemic antibiotics often fail to achieve adequate local therapeutic antibiotic levels around the implants due to tissue trauma and disrupted blood circulation [13]. Further, the typical administration of relatively high doses of antibiotics for bacterial eradication may promote bacterial resistance, rendering the infection treatment ineffective [4].

In recent years, there is a growing interest in introducing safe and efficient antibiofilm strategies for overcoming the limitations of systemic antibiotic treatment options. A promising strategy is the prevention of early-onset infections by inhibiting initial bacteria attachment and colonization on the implants during the implantation surgeries [1,6,13,17]. In addition to implant surface modification for effectively averting biofilm formation, implant coatings with antibacterial and bone integration properties are attractive therapeutic options for use [4–6,16,18]. However, it is important addressing different drawbacks of existing polymeric and composite antibacterial coatings in orthopedic surgeries, including toxic side effects, long-term instability, and limited effectiveness [5,7,11,19–26]. Safe and biocompatible materials are attractive for use in the development of antibacterial coatings. Among these materials, omega-3 polyunsaturated fatty acids (ω-3 PUFAs), including eicosapentaenoic (EPA) and docosahexaenoic (DHA) acids, have health promoting effects, including antibacterial and antibiofilm activities against various bacterial pathogens [9,12,15]. Further, these bioactive lipids have anti-inflammatory activities, and they may promote the bone health through minimizing the risks of osteoporosis [2,6,15,27–29]. In a recent study [30], we reported on the inherent antibacterial and antibiofilm activities of antibiotic-free nano-self-assemblies (hexosomes and vesicles) loaded with DHA against *S. aureus* and *S. epidermidis*, which are among the major microorganisms associated with the development of biofilm infections on medical devices.

Non-lamellar lyotropic liquid crystalline (LLC) phases are attractive for use in design of coatings owing to their inherent unique structural architectures and their loading and sustaining drug release properties [31–33]. In a recent study, we reported on the antibacterial and antibiofilm activities of colistin-loaded inverse bicontinuous *Pn3m* nanostructures (double diamond phases) coated on model orthopedic implants against *Pseudomonas aeruginosa* [34]. Here, it is worth noting that new ω-3 PUFA monoacylglycerols (such as MAG-DHA) are attractive for use in designing liquid crystalline coatings owing to their tendency to display inverse hexagonal (H_2) phases on exposure to excess water [35,36]. Further, they have health promoting effects and they may find applications in treatment of different disorders, including cancer [37–39]. It was, therefore, our interest to use binary combinations of MAG-DHA and GMO for designing structurally tunable antibacterial coatings and assess their potential antibiofilm activities.

It is the first report to our knowledge on the development of antibiotic-free non-lamellar liquid crystalline coatings for preventing biofilm formation on model orthopedic implants. In this work, we focus on the role of lipid composition on modulating the structural features of the produced surface patterns on the implants and their antibacterial activities against two common biofilm-forming bacteria *S. epidermidis* 5D and *S. aureus* ATCC 29213. In the characterization studies, SAXS experiments were conducted to gain insight into the structural features of already prepared coatings; whereas the dynamic self-assembly behavior of both lipids (MAG-DHA and GMO) during the coating production was investigated by *in situ* GISAXS.

2. Materials and methods

2.1. Materials

Docosahexaenoic acid monoacylglycerol (MAG-DHA; >99% of purity) was purchased from Larodan (Solna, Sweden). Capmul GMO-90 EP/NF (mainly consisting of glycerol monooleate and therefore referred below as GMO) was kindly donated by Abitec Co. (Columbus, USA). This commercial distilled monoacylglycerol product consists of

monoglycerides (97%, mainly GMO (88.5%)), and diglycerides (~2.7%). Tryptic soya broth (TSB) was purchased from Oxoid (Roskilde, Denmark). Luria-Bertani (LB) broth and the agar plates were supplied by the Department of Immunology and Microbiology (Substrate and Sterile Centre, University of Copenhagen). In addition to NaOH pellets (>99% purity), the organic solvents ethanol absolute (>99.8% purity) and acetone (>99.5% purity) were purchased from Sigma-Aldrich (Darmstadt, Germany). 10 mM phosphate buffered solution (PBS, pH 7.4) was prepared from the following salts: sodium chloride (8 g/L), potassium chloride (0.2 g/L), sodium phosphate dibasic dihydrate (1.8 g/L), and potassium phosphate monobasic (0.245 g/L). These salts were purchased from Sigma-Aldrich (Darmstadt, Germany). All chemicals were of analytical grade and used without further purification. Regular stainless-steel discs (SS) with a diameter of 15 mm and a thickness of 0.3 mm were purchased from Holzura (Wuppertal, Germany) and used as model metallic implants. *p*-type silicon wafers (Si-wafers) with dimensions of 20 mm × 15 mm were purchased from Ossila Ltd. (Sheffield, UK) and used in the GISAXS study.

2.1.1. Preparation of fully hydrated LLC phases

The LLC phases were prepared in excess buffer (10 mM PBS, pH 7.4) at different lipid compositions as recently described [34]. Briefly, an ethanol stock solution of MAG-DHA was prepared at MAG-DHA/ethanol weight ratio of 60:40. At appropriate amounts, melted GMO was then added to produce ethanol solutions of MAG-DHA/GMO at the following MAG-DHA/GMO volume ratios: 63:37, 36:64, and 16:84. Ethanol stock solution of GMO alone was also prepared as described above. For vaporization of ethanol, these solutions containing GMO, MAG-DHA, or binary MAG-DHA/GMO mixtures were left for drying under vacuum by using PELCO® Mini Hot Vac Desiccator (California, USA). Then, the produced dry lipid films were exposed to 2 mL of 10 mM PBS (pH 7.4), and the samples were kept rotating by using Intelli-mixer rotorarm (Riga, Latvia) at room temperature (RT) for at least 72 h prior to SAXS characterization studies.

MAG-DHA is highly susceptible to oxidation; it was therefore important to conduct all investigations on fresh coatings. The dry lipid films were also flushed with nitrogen gas and incubated in the dark at 4 °C before use. It is worth also noting that the antibacterial activities of the coatings were also tested on dry films left for prolonged period at 4 °C. There was no indication of any decrease in their antibacterial efficacy (data not shown).

2.1.2. Structural characterization of LLC phases by small angle x-ray scattering (SAXS)

In addition to the described below *in situ* out-of-equilibrium GISAXS experiments on coatings, it was important to conduct SAXS experiments. It was our interest to gain insight into the influence of the lipid composition on the structural features of the already prepared LLC phases based on MAG-DHA or its binary combination with GMO under full hydration conditions. The SAXS measurements were conducted at RUCSAXS (Roskilde University Interdisciplinary X-ray Scattering Hub, Roskilde, Denmark) with a Xenocs Xeuss 3.0 UHR XL instrument (Grenoble, France) equipped with an Eiger 2R 1 M detector from Dectris (Baden, Switzerland). The source is a Xenocs GeniX 3D Cu-Kα HFVL X-ray tube with focusing optics and X-ray wavelength of 1.54 Å. The sample-to-detector distance was 600 mm (calibrated with a silver behenate standard). The scattering vector ($q = (4\pi/\lambda)\sin(\theta)$, where λ and θ are the wavelength and the scattering angle, respectively) was in the range of 0.5–4.0 nm^{-1}. The fully hydrated LLC phases were mounted in sandwich sample holders with both sides of each spacer disk covered with Kapton foils. Eight samples with a thickness of 1 mm were mounted in the sample holder in a 4 × 2 array. All measurements were performed at 37 ± 1 °C using a Julabo Dyneo water circulator (Seelbach, Germany).

The recorded 2D SAXS data were analyzed with BioXTAS RAW 2 [40]. They had been background (scattering from an empty cell with Kapton windows) subtracted after the employed azimuthal averaging. Lorentzian fitting was then employed to determine the *q*-values of the detected Bragg peaks. The interplanar distance, *d*, for each peak was calculated and used to determine the corresponding lattice parameters of the identified LLC phases (H_2 and *Pn3m* nanostructures). In line with previous studies on the behavior of different monoacylglycerols, the SAXS patterns of the inverse micellar solution (L_2 phase) displayed single broad peaks [32,36,41].

The characteristic distances ($d = \frac{2\pi}{q}$) of these L_2 phases were calculated. Further, the lattice parameters of the non-lamellar phases (H_2 and cubic *Pn3m* self-assemblies), respectively, were calculated by using the following equations [42,43]:

Lattice parameter of the H_2 phase:

$$a = \frac{4\pi}{q_{hkl}\sqrt{3}}\sqrt{h^2 + hk + k^2} \quad (1)$$

Lattice parameter of the cubic *Pn3m* phase:

$$a = \frac{2\pi}{q_{hkl}}\sqrt{h^2 + k^2 + l^2} \quad (2)$$

where q_{hkl} is the length of the scattering vector and *h*, *k*, and *l* are the Miller indices of the detected Bragg peaks.

2.1.3. Dry lipid film coating preparation

Before employing the lipid coating procedure, the SS discs were cleaned in an ultrasonic cleaner (Branson Ultrasonics, Connecticut, USA) for 10 min by sequentially using acetone, ethanol, and deionized water (DI). Then, the discs were sonicated in 5 M NaOH aqueous solution for 30 min, rinsed with DI water, and kept in ethanol until use. To dry these cleaned discs, an air stream was used at RT. The same protocol was used for Si-wafers, however, these were stored in acetone after the surface cleaning procedure. Then, they were coated through directed self-assembly of MAG-DHA alone or its combination with GMO on their surfaces.

The dry lipid film coatings were prepared as recently described [34]. The ethanol solutions of MAG-DHA alone, GMO alone, and their binary mixtures (at MAG-DHA/GMO volume ratios of 63:37, 36:64, and 16:64) were prepared as described above. 40 μL of these solutions were used to coat the SS discs by using a spin coater (Mutech μcoater, Bariloche, Argentina) for 20 s at 4000 rpm. Then, the coated discs were left for drying overnight to remove ethanol and subsequently used in the employed antibacterial activity assays. The same procedure has been employed to produce dry lipid films on Si-wafers for the *in situ* GISAXS out-of-equilibrium structural characterization study. To minimize the background scattering, Si-wafers are preferred as substrates for grazing incidence X-ray studies. They have excellent optical properties and ultra-low surface roughness [44,45].

2.1.4. In situ synchrotron grazing incidence small-angle X-ray scattering (GISAXS) study for real-time monitoring of hydration-induced production of LLC coatings

The exposure of the dry lipid films coated on the SS discs to bacteria suspensions, as described below, leads to their simultaneous hydration. With an attempt at mimicking the conditions and gaining insight into the hydration-mediated formation of inverse LLC phases or micellar solutions, a set of *in situ* GISAXS experiments were conducted. In this study, dry lipid films of MAG-DHA alone (or GMO alone) and their binary combinations were coated on Si-wafer surfaces. The employed GISAXS set-up is shown in Fig. 1.

In GISAXS investigations, a monochromatic X-ray beam typically hits the sample at a low angle (in the range of 0.10–0.50°) around the critical angle for total reflection [46,47]. A 2D detector measures the scattered photon intensity in the directions parallel (q_y) and perpendicular (q_z) to the sample surface [46,48]. From the obtained 2D image on the reciprocal space, it is possible to identify the sample's structure [49,50]. In

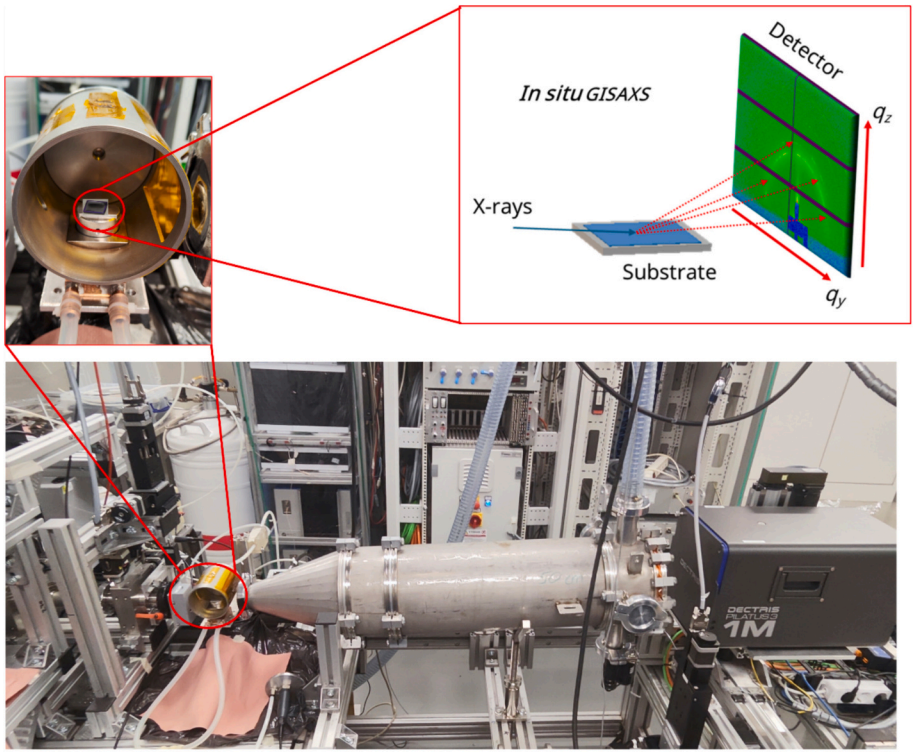

Fig. 1. The employed *in situ* GISAXS set-up for monitoring in real-time the structural alterations occurring during hydration-mediated formation of inverse self-assemblies (L_2, H_2, and cubic nanostructures). The GISAXS experiments were conducted by exposing the dry lipid films coated on Si-wafers to air with different relative humidity (RH) levels at RT by using a supersonic humidifier. The grazing incidence angles used in the experiments ranged from 0.35° to 0.47°.

this study, the GISAXS measurements were conducted at the Austrian SAXS beamline at Elettra Synchrotron (Trieste, Italy) [51]. The sample-to-detector distance was 1217 mm, resulting in a q-range of 0.5 nm^{-1} < q < 5.5 nm^{-1}. As depicted in Fig. 1, the dry lipid film coated substrate (Si-wafer) was placed in a metallic custom-made humidity chamber, which was equipped with two Kapton windows with a thickness of 13 μm to allow pass through the incident and the scattered beam. The wavelength, λ, was 0.154 nm, and the 2D GISAXS patterns were collected with a Pilatus3 1 M detector (Dectris, Baden, Switzerland) at a specific grazing angle. The angular scale of the detector was calibrated with silver behenate. The measurements were conducted at different relative humidity (RH) levels. At any given temperature, the RH is defined as the ratio of the actual water vapor pressure to the water vapor pressure under saturation conditions. In this study, a custom-made setup, consisting of an ultrasonic humidifier and two RH sensors, was employed to precisely regulate the RH level by mixing highly humidified air (>95% RH) with dry air (<3% RH) in a pre-chamber before delivering into the humidity chamber. A humidity sensor, which was coupled with a proportional-integral-derivative (PID) controller, maintained the target RH level, while a secondary sensor in the humidity chamber monitored the RH levels during X-ray irradiation. Further detailed information on the used chamber is presented in the previous report of Sharifi et al. [52]. The GISAXS experiments were conducted by gradually increasing the RH level from 15% to 95% at a controlled rate of 1% / min (with deviation <1%). The X-ray exposure time was 2 s every 2 min. Additional experiments were conducted for 30 min at the highest RH level (95%) with an X-ray exposure time of 2 s every 2 min to further investigate the effect of hydration on the structural features of the films. The recorded 2D GISAXS diffraction patterns were radially integrated with the data reduction pipeline available at the SAXS beamline [53] to obtain the scattering vector (Intensity, I_q). The resulting 1D curves were further analyzed with BioXTAS RAW 2 [40] to identify the phases and determine the lattice parameters and the characteristic distances of the inverse LLC phases and inverse micellar solutions (L_2 phases), respectively. The peak positions were analyzed using the standard Born approximation (BA). Since the grazing incident angles (ranging from 0.35° to 0.47°) were sufficiently larger than the critical angle for Si-wafer (≈ 0.22°), the distorted wave Born approximation (DWBA) corrections for refraction could be neglected, as already reported by Rittman et al. [54]. Due to the difficulty in thermostating the investigated coatings at 37 °C, when varying the humidity level, the GISAXS experiments were only conducted at 25 °C.

2.1.5. Bacterial strains and growth conditions

The overnight cultures of *S. aureus* ATCC 29213 and *S. epidermidis* 5D strains were prepared by transferring a loop of frozen bacteria to 5 mL TSB media. At 37 °C, they were shaken overnight at 160 rpm by using IKA HS 501 orbital shaker (Staufen, Germany). Prior to the antibacterial activity evaluation, the bacterial cultures (≈10^9 Colony Forming Unit (CFU)/mL) were diluted in TSB medium to obtain a bacterial suspension of ≈10^5 CFU/mL.

2.1.6. In vitro antibacterial activities of the LLC coatings based on MAG-DHA and MAG-DHA/GMO binary mixtures

The coated SS discs with dry lipid films were incubated at 37 °C in 12-well microtiter plates (Greiner Bio-One GmbH, Kremsmünster, Austria), containing 1 mL of *S. aureus* ATCC 29213 (or *S. epidermidis* 5D) suspension with ≈10^5 CFU/mL. They were then shaken at 160 rpm for 24 h by using IKA HS 501 orbital shaker (Staufen, Germany). To determine the antibacterial activities of the hydration-mediated LLC coatings after 24 h of incubation of the dry lipid films in the bacterial suspensions, 100 μL of these suspensions was then subsequently transferred to a 96-well microtiter plate, and the optical density was measured at 600 nm (OD600) by using PerkinElmer 2030 Multilabel Reader VICTOR X4 UV-spectrophotometer (Shelton, USA). In this study, the coated SS discs (n = 3) with dry GMO films and overnight bacterial cultures of *S. aureus* ATCC 29213 and *S. epidermidis* 5D were used as controls (n = 3).

2.1.7. Time-kill assay

Dry lipid films of MAG-DHA and MAG-DHA/GMO binary coatings (produced at MAG-DHA/GMO volume ratios of 63:37, 36:64, and 16:64) coated on SS discs were prepared as described above. They were incubated in bacterial suspensions of *S. aureus* ATCC 29213 and *S. epidermidis 5D* at 37 °C and shaken at 160 rpm. The conducted time-kill experiments were performed to evaluate the antibacterial activities of the coatings at different post-incubation time points (0 min, 15 min, 30 min, 1 h, 2 h, 4 h, 6 h, and 24 h). In this study, 50 μL of the incubation medium was collected at these time points and subsequently serially diluted in 0.9% (*w/v*) sterile saline solution to achieve appropriate concentrations for CFU counting. 10 μL of the last 3 dilutions were plated on LB agar and incubated overnight at 37 °C. Then, the formed colonies were counted and expressed as $\log_{10}$ CFU/mL. The killing curves were obtained by plotting the colony count ($\log_{10}$ CFU/mL) as a function of time. In this study, the bacterial cultures *S. aureus* ATCC 29213 and *S. epidermidis* 5D, which are kept overnight, were used as controls.

2.1.8. Data analysis

All experiments were conducted in triplicates, and the analysis was done by one-way ANOVA test. $p < 0.05$ was statistically considered significant. Each value is presented as mean ± standard deviation (SD). MS Excel 365 was used for plotting the graphs and performing statistical analysis.

3. Results and discussion

3.1. Structural characterization of fully hydrated self-assemblies: SAXS study

To gain insight into the structural features of the fully hydrated LLC phases generated from MAG-DHA alone, GMO alone, and binary MAG-DHA/GMO mixtures (at MAG-DHA/GMO volume ratios of 63:37, 36:64, and 16:64), SAXS experiments were conducted at 37 °C. The SAXS curves are shown in Fig. 2, and the calculated lattice parameters of the identified inverse LLC phases are presented in **Table 1**. In line with previous studies [32,35,36,55,56], MAG-DHA and GMO tend to display inverse H_2 and bicontinuous double-diamond cubic phases (crystallographic space group: *Pn3m* (Q^{224})), respectively (Fig. 2, red and black SAXS patterns, respectively). The lattice parameters of these H_2 and cubic *Pn3m* phases were 4.50 and 8.71 nm, respectively (**Table 1**). As shown in Fig. 2, combining MAG-DHA with GMO led in a lipid composition-dependent manner to a phase transition in the following order: a neat H_2 phase → biphasic feature of two coexisting H_2 phases + H_2 phase → cubic *Pn3m* phase. The identification of the H_2 phase was based on the detection of its first three characteristic Bragg peaks with distinct spacing ratios of $\sqrt{1}:\sqrt{3}:\sqrt{4}$; whereas the first six

Table 1
Structural parameters of already prepared fully hydrated LLC phases (SAXS analysis), and phases identified at different lipid compositions and employed RH levels (the out-of-equilibrium GISAXS study). The SAXS and GISAXS experiments were conducted at 37 and 25 °C, respectively.

Lipid composition	*In situ* GISAXS results				SAXS findings	
	Conditions	Phase	*d*, nm	*a*, nm	Phase	*a*, nm
MAG-DHA	RH: 15%	L_2	2.77	–	H_2	4.50
	RH: 95%	L_2	3.20	–		
	RH: 95% (after 30 min)	L_2	3.25	–		
MAG-DHA/GMO (63:37)	RH: 15%	L_2	2.96	–	H_2	5.04
	RH: 95%	L_2	3.53	–		
	RH: 95% (after 30 min)	H_2	–	4.12		
MAG-DHA/GMO (36:64)	RH: 15%	L_2	3.09	–	H_2	5.55
	RH: 95%	H_2	–	4.25		
		H_2	–	4.63		
	RH: 95% (after 30 min)	H_2	–	4.36	H_2	5.34
MAG-DHA/GMO (16:84)	RH: 15%	L_2	3.11	–		
		L_c	–	–		
	RH: 95%	*Ia3d*	–	9.34	*Pn3m*	7.91
	RH: 95% (after 30 min)	*Ia3d*	–	9.50		
GMO	RH: 15%	L_2	3.31	–		
		L_c	–			
	RH: 95%	*Ia3d*	–	10.12	*Pn3m*	8.71
	RH: 95% (after 30 min)	*Ia3d*	–	10.23		

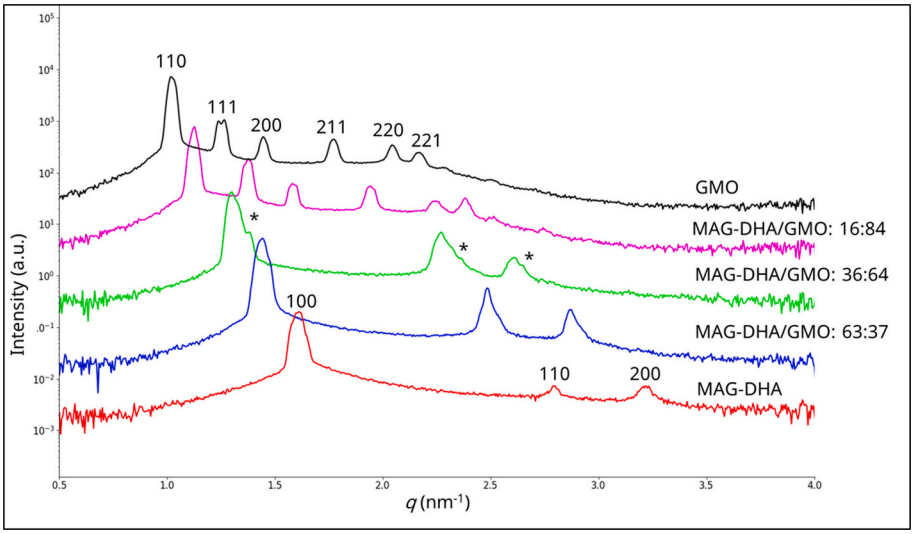

Fig. 2. Effect of lipid composition on the structural features of the fully hydrated LLC phases at 37 °C. These self-assemblies were produced on exposure of single amphiphiles (MAG-DHA (red) and GMO (black)) and three of their binary combinations to excess PBS (pH 7.4). These binary mixtures were prepared at MAG-DHA/GMO volumetric ratios of 63:37 (blue), 36:64 (green), and 16:64 (purple). At a MAG-DHA/GMO ratio of 36:64, the SAXS curve (green) indicated the formation of a biphasic feature of two coexisting H_2 phases. The detected peaks characteristic for the second H_2 phase are marked with an asterisk (*). The scattering intensity was scaled by an arbitrary constant for better visibility. (For interpretation of the references to colour in this figure legend, the reader is referred to the web version of this article.)

characteristic Bragg peaks of the cubic *Pn3m* phase had distinct spacing ratios of $\sqrt{2}:\sqrt{3}:\sqrt{4}:\sqrt{6}:\sqrt{8}:\sqrt{9}$ [35,55,57–60]. 2D SAXS images of fully hydrated LLC bulk phases at 37 °C are presented in *Supporting Information, **Fig. S1***. They prepared using binary MAG-DHA/GMO mixtures at the following MAG-DHA/GMO ratios: 63:37, 36:64, and 16:84.

3.2. Real-time monitoring of hydration-induced production of LLC coatings: In situ GISAXS study

In addition to SAXS characterization studies, it was important for evaluating the antibacterial activities of the self-assembled nanocoatings to mimic the biological milieu and gain insight on the hydration-induced dynamic self-assembly on exposure of the dry lipid films coated on model implants to the bacterial suspensions. Therefore, a set of GISAXS experiments were conducted at 25 °C. It is worth noting that SAXS in transmission geometry is not optimal for studying nanostructured surfaces and thin films. This is due to the X-ray absorption of the substrate (Si-wafer) and the presence of very small volume in the thin lipid film's geometry, hindering a successful data analysis with acceptable signal to noise ratio. To overcome such limitations, there is a growing interest in conducting GISAXS experiments at equilibrium and out-of-equilibrium conditions [47,61,62]. By performing small-angle scattering experiments in a reflection geometry using an X-ray beam with an angle of typically ~0.1–0.5°, the large footprint of the beam on the sample significantly increases the illuminated sample volume. Likewise, the substrate's absorption is avoided, when analyzing the scattering of the beam reflected from the sample and the substrate surface [62]. In this study, the GISAXS measurements were performed at grazing incidence angles of 0.47°, 0.44°, 0.36°, 0.47°, and 0.35° for MAG-DHA alone, binary MAG-DHA/GMO mixtures at ratios of 63:37, 36:64, 16:64, and GMO alone, respectively.

It is worth noting that technical limitations hampered direct comparison of SAXS and GISAXS results. It was not possible to conduct the GISAXS experiments at 100% RH, and it was not feasible to mimic the physiological conditions and conduct them under full hydration and equilibrium conditions. Further, it was not feasible to conduct the *in situ*

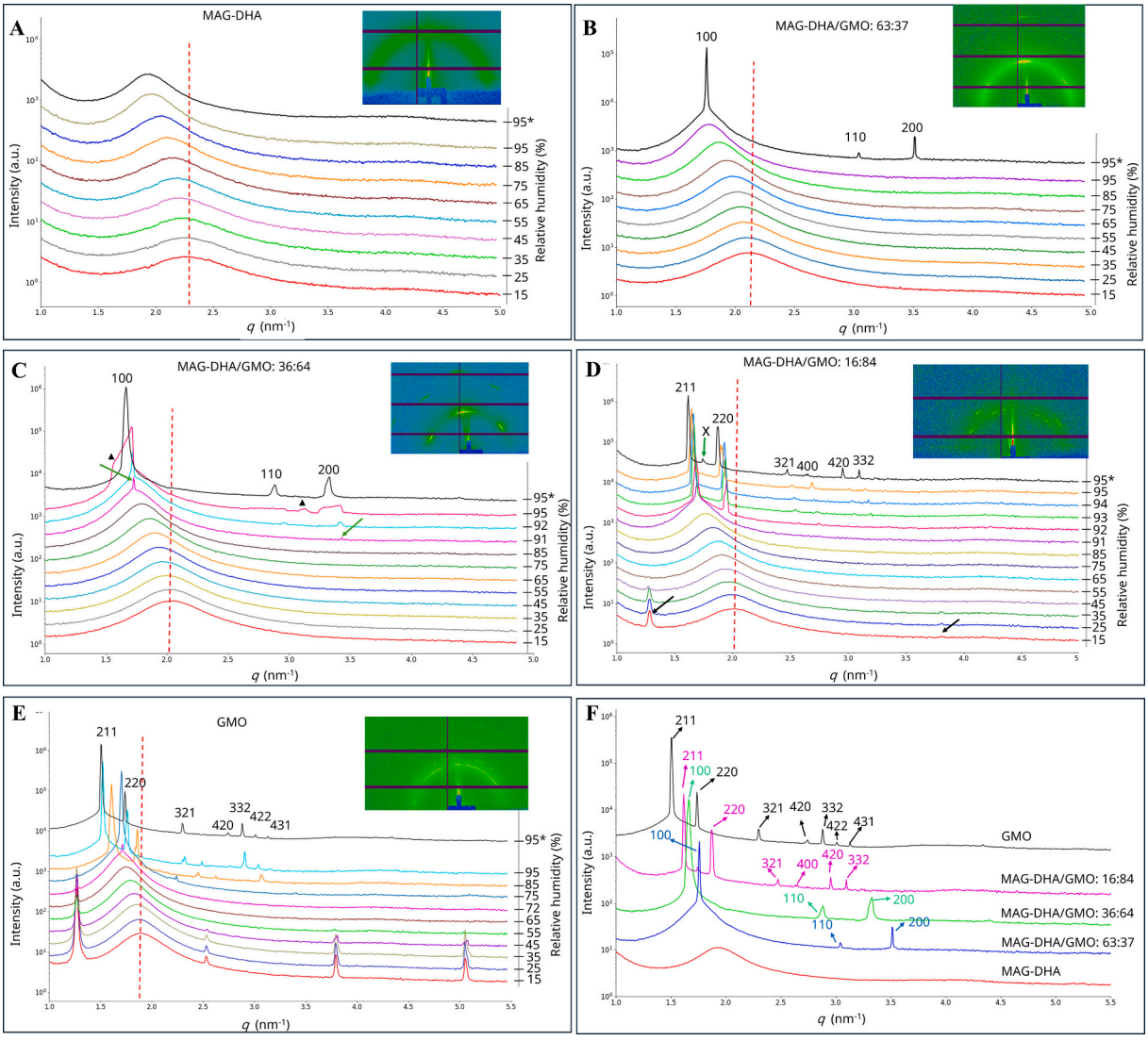

Fig. 3. GISAXS patterns (I–*q*) of films prepared with MAG-DHA alone (A), MAG-DHA/GMO binary systems at ratios of; 63:37 (B), 36:64 (C), 16:84 (D), and GMO alone (E). They were obtained under constantly increasing RH level and after 30 min of incubation at 95% RH (marked with an asterisk). At all investigated lipid compositions and the highest RH level of 95%, the patterns are shown after 30 min of incubation in the humidity chamber (F). Further, the corresponding 2D GISAXS maps of the films (corresponding to the patterns marked with an asterisk are shown (see insets, Fig. 3A-E). To guide the eye, red vertical dashed lines are given in Fig. 3A-E to show the influence of hydration (by augmenting the RH level) on swelling of the inverse micellar L_2 phases (shifting the single broad peaks to lower *q* values) and induction of transitions from L_2 phases to non-lamellar liquid crystalline phases. These phase transitions are detected upon partial replacement of MAG-DHA by GMO. (For interpretation of the references to colour in this figure legend, the reader is referred to the web version of this article.)

GISAXS studies at 37 °C and use PBS (pH 7.4). Regarding the effect of the aqueous medium composition on the structural features of the self-assemblies, we do not expect that the dissolved ions in the buffer would affect the structural features of the coatings, as the membranes based on GMO alone, MAG-DHA alone, or their binary combinations are electrically neutral.

In the initial time-resolved GISAXS experiments, the structural features of the dry MAG-DHA film coated on a Si-wafer were investigated at RT by augmenting the RH level from 15% to 95% at a rate of 1%/min. At the lowest investigated RH level (15% RH), a single broad peak at q value of about 2.27 nm^{-1} was detected (a corresponding characteristic distance, d, value of 2.77 nm). This detected broad peak was shifted to lower q values on augmenting the RH level (15% < RH ≤ 95%)(Fig. 3A). At 95% RH, the detected broad peak had $q \approx 1.93$ nm^{-1} (a corresponding d value of 3.25 nm). There were no indications of any hydration-induced structural transitions after 30 min at 95% RH (***Fig. S2A***, *Supplementary Information*). The characteristic distances of the identified L_2 phases and the lattice parameters of cubic and H_2 phases are given in **Table 1**.

The obtained GISAXS map most likely indicates hydration-induced swelling of the L_2 phases on increasing the RH level (Fig. 3A). This is in line with previous studies on the tendency of MAG-DHA and other ω-3 PUFA monoacylglycerols (including docosapentaenoic acid (MAG-DPA) and eicosapentaenoic acid (MAG-EPA) to display inverse micellar solutions (L_2 phases) under limited hydration conditions [35,36]. At a water content of 15.0 wt%, the reported characteristic distances of the L_2 phases of MAG-DHA and MAG-EPA were 3.30 and 3.58 nm, respectively [35,36]. It was also reported on direct L_2-H_2 phase transitions on significantly augmenting the solubilized water content in samples based on MAG-DHA, MAG-DPA, or MAG-EPA [36]. Thus, it was evident from the formation of the L_2 phases that the employed experimental time of 30 min at the highest RH level of 95% was not sufficient to trigger a significant increase in water uptake, and therefore a transition from swollen micelles to H_2 phase was not detected (Fig. 3F, the red colored GISAXS pattern).

As the lipid composition plays an important role in modulating the structural features of self-assemblies, it was worth conducting the GISAXS experiments on films produced from binary mixtures of MAG-DHA and GMO. At MAG-DHA/GMO volume ratio of 63:37 (Fig. 3B), increasing the RH level led to a hydration-induced swelling of the L_2 phase: augmenting the RH level from 15% to 95% was associated with an increase of about 20% in the characteristic distance of the L_2 phase (**Table 1**). At the highest RH level (95%), the time-resolved GISAXS measurements indicated the persistence of the broad peak, but it continued to shift to lower q values under initial conditions (<4 min). After 4 min, a newly formed coexisting H_2 phase with lattice parameter, a, of 4.12 nm was started to evolve and its first two characteristic peaks (100 and 200 reflections) were detected at $q \approx 1.77$ nm^{-1} and $q \approx 3.52$ nm^{-1} (corresponding spacing ratios of $\sqrt{1}$ and $\sqrt{4}$, marked with black arrows, ***Fig. S2B***). The lattice parameter of this coexisting H_2 phase was unchanged on increasing the time up to 30 min. Further, an additional characteristic peak with a spacing ratio of $\sqrt{3}$ started to emerge after 10 min (this peak is marked with red arrow, ***Fig. S2B***).

A similar behavior, including the induction of L_2-H_2 phase transition, was detected at a higher GMO content (MAG-DHA/GMO volume ratio of 36:64). However, two characteristic peaks of the H_2 phase (at $q \approx 1.73$ nm^{-1} and $q \approx 3.43$ nm^{-1}, marked with green arrows, Fig. 3C) with $a =$ 4.21 nm started to evolve at a lower RH level (91%). A further increase in the RH level to 95% led to formation of H_2 phase with corresponding characteristic peaks at q values of 1.71 nm^{-1} and 3.41 nm^{-1}, respectively ($a =$ 4.25 nm, Fig. 3C). However, the GISAXS map indicated the structural heterogeneity of the film as a second coexisting H_2 phase with two characteristic peaks was detected at q values of 1.57 nm^{-1} and 3.13 nm^{-1} (marked with a triangle, Fig. 3C). ***Fig. S2C*** shows the obtained 2D GISAXS map within 30 min of incubation of the dry film in the humidity chamber at RH of 95%. The coexisting second H_2 phase had vanished, and the time-resolved GISAXS investigations indicated transition from a neat H_2 phase with a lattice parameter of 4.44 nm after 2 min to a biphasic feature of two coexisting H_2 phases at different time points between 4 and 28 min (***Fig. S2C***). The lattice parameters of these two phases were 4.45 and 4.57 nm at 4 min (***Fig. S2C***). These time-dependent structural alterations are most likely attributed to a slight increase in the hydration level of the produced liquid crystalline phases. After 30 min of placement of the film in the humidity chamber at RH of 95%, a neat H_2 phase with $a =$ 4.36 nm was detected (Fig. 3C).

Hydration-induced generation of inverse bicontinuous phases occurs at relatively high content of GMO. At MAG-DHA/GMO ratio of 16:84 and 15% RH, the GISAXS pattern of the film, similar to the aforementioned patterns, displays a single broad peak with $q \approx 2$ nm^{-1} (corresponding to d value of 3.11 nm). Further, two additional peaks (first and fourth characteristic peaks of a solid crystalline (L_c) phase with q values of approximately 1.29 nm^{-1} and 3.81 nm^{-1}, marked with black arrow, Fig. 3D) were detected. The latter phase with a lattice parameter of 4.88 nm may contain a residual amount of ethanol. It started to vanish at around 50% RH. In addition to the gradual water-swelling behavior of the micellar phase at 15% < RH ≤ 90%, an additional liquid crystalline phase started to be developed at RH of 91% RH. Its first peak was detected at $q \approx 1.69$ nm^{-1}, and an additional peak with $q \approx 1.94$ nm^{-1} was detected on increasing RH level to 92% and 93% (Fig. 3D). Both peaks are characteristic for an inverse bicontinuous gyroid cubic phase (crystallographic space group: *Ia3d* (Q^{230})). At RH of 95%, four additional characteristic peaks were detected. The q values of all peaks were 1.65, 1.90, 2.51, 2.70, 3.01 and 3.15 nm^{-1}, indicating the generation of cubic *Ia3d* phase with a of 9.34 nm. The diffraction peaks further shifted to lower q values as evident from the time-resolved GISAXS investigations at 95% RH (***Fig. S2D***). After 30 min, the hydration of the film induced a slight increase in the lattice parameter of the cubic phase to 9.50 nm (***Fig. S2D***). It is worth noting that the GISAXS patterns presented in ***Fig. S2D*** and Fig. 3D indicated the coexistence of an unidentified phase (denoted as phase X, marked with green arrow). Considering the tendency of MAG-DHA to display an inverse H_2 phase, it is not excluded that traces of H_2 phase with a of about 4.2 nm are still present in the hydrated film. The GISAXS analysis indicates, therefore, that the interplay of hydration timescale and employed experimental sample environment (see the discussion below) plays a crucial role in modulating the structural features of the inverse self-assemblies and dictating the phase transitions. As compared to SAXS experiments conducted on the samples under full hydration and equilibrium conditions, the detection of phase X in the out-of-equilibrium GISAXS investigations is most likely attributed to presence of kinetically trapped intermediate structures that may lose their stability upon prolonging the exposure time at RH of 95%. In the absence of MAG-DHA, the sole GMO film displays an inverse cubic *Ia3d* phase at relatively high RH levels (≥75%). In line with the behavior described above, the L_c phase with 4 characteristic peaks at 1.26, 2.53, 3.79 nm^{-1} and 5.05 was detected together with a micellar phase having a single broad peak at $q \approx 1.90$ nm^{-1} ($d =$ 3.31 nm) at RH 15%. As shown in Fig. 3E, increasing the RH level (15% < RH ≤ 95%) was associated with disappearance of this crystalline phase, swelling of the micellar phase (***Fig. S2F***), and appearance of the cubic *Ia3d* phase. At 95% RH, a neat cubic *Ia3d* phase with at least 6 characteristic peaks at q values of 1.52, 1.76, 2.32, 2.49, 2.90 and 3.04 nm^{-1} was generated. Its lattice parameter was very slightly increased from 10.12 nm to 10.23 nm after 30 min of the film's placement in the humidity chamber (***Fig. S2E***). These results are consistent with those recently reported on the tendency of GMO to display coated cubic *Ia3d* phases with a lattice parameter around 11.5 nm at relatively high RH levels (RH ≥ 85%).

In our study, there was no indication of formation of inverse cubic *Pn3m* and H_2 phases at the employed RH levels on exposure of dry films of GMO alone, or MAG-DHA alone, respectively (Fig. 3F, **Table 1**). This is consistent with previous studies [35,36,55,63,64]. Duration with a longer incubation time is most likely needed to induce the generation of

these self-assemblies. For instance, cubic *Pn3m* phases were produced after 3 h of incubation of dry GMO films coated on Si-wafers in excess buffer [63]. Here, it is also worth noting that the water swelling rate of dry films of lipids with propensities to display inverse bicontinuous cubic or H_2 phases (such as GMO

and MAG-DHA) is most likely affected by the employed experimental sample environment. In contrast to most studies, typically reporting on the structural features of films produced at a constant water-to-lipid ratio, which are placed in a closed cell or immersed in an aqueous environment, our GISAXS investigations were conducted in an open environment with humidity control (Fig. 1) that may decrease the water uptake by the dry lipid films within the investigated incubation time. In addition, difficulties in a precise control of the humidity level [54,65] may affect the water swelling rate and the dynamic self-assembly behavior. At very high RH levels in the range of 96–98%, it was reported using humidity scanning quartz crystal microbalance with dissipation (HS-QCM-D) on hydration-induced liquid crystalline lamellar phase (L_α)-cubic *Pn3m* phase transition [66,67]. It is also worth considering the following plausible factors that may affect GISAXS patterns: orientation of the liquid crystalline domains, variations in the film thickness and morphology (depending on coating composition and the employed coating method), and the choice of the substrate surface and its treatment (cleaning) and interactions with the self-assembled layers [47,68–70].

3.3. Antibacterial activities of nanostructural coatings based on MAG-DHA alone and its combination with GMO

The antibacterial activities of monoacylglycerols can be more potent (up to 200 times) than their corresponding free fatty acids (FFAs) [71–75]. It was, therefore, of our interest to evaluate the antibacterial activities of a set of coatings produced using two single monoacylglycerols (MAG-DHA and GMO) and three of their binary combinations (prepared at MAG-DHA/GMO volume ratios of 63:37, 36:64, and 16:84). In this study, the five families of antibiotic-free simple-by design LLC coatings were tested against *S. aureus* ATCC 29213 and *S. epidermidis* 5D strains, which represent the most common bacterial species causing orthopedic joint infections [25,26,76]. As shown in Fig. 4, our results indicated unique inherent antibacterial activities of the coatings based on MAG-DHA alone and those based on binary MAG-DHA/GMO combinations of 63:37 and 36:64 against both strains. This was evident by a complete bacterial eradication after 24 h of incubation of the corresponding dry lipid films coated on SS discs in the bacteria suspensions. The control coating produced using GMO alone, and that produced at MAG-DHA/GMO 16:84 did not exhibit any antibacterial inhibition. Thus, these results suggest that MAG-DHA plays a decisive role in the mode of action in targeting the bacterial cytoplasmic membrane. Here, the nature of this ω-3 PUFA monoacylglycerol most likely plays an important role in disrupting the structural features of the bacterial membranes, leading to variations in their lipid compositions, fluidities, and their membrane permeabilities, which eventually result in the bacterial cell death. Clearly, our findings indicate that the monoacylglycerol form of DHA retains its potent antibacterial activity, and, therefore, the findings are in line with different studies in the literature, reporting on the potent antibacterial activity of DHA against the Gram-positive bacteria *S. epidermidis* and *S. aureus* [2,8,15,30]. In addition to the reported beneficial health effects of MAG-DHA (including anticancer and anti-inflammatory properties, and high DHA bioavailability) [37,77–80], this study reports for first time to the best of our knowledge on the strong antibacterial activity of this specific bioactive lipid.

Like other ω-3 PUFA monoacylglycerols [78–80], MAG-DHA most likely acts as a safe precursor for generating DHA derivatives, which may play an important role in mediating the antibacterial activity on exposure of MAG-DHA to bacteria. It is worth noting that the mechanism of action of DHA and other ω-3 PUFAs is still unclear. The proposed multiple mechanisms on how ω-3 PUFAs can target bacterial cell membranes for exerting their antibacterial effects are presented in Fig. 5. These essential fatty acids exhibit a membrane-lytic behavior owing to their nature [72,81,82]. Therefore, their interactions with bacteria can induce a disruption of bacterial membranes, leading eventually to their destabilization through most likely a pore formation mechanism. These significant structural alterations in the bacterial membrane's structure can also be associated with disrupting key biological processes, including the electron transport chain and the oxidative phosphorylation, which are essential for energy production in bacterial cells [2,81,82]. Further, it was reported that ω-3 PUFAs can inhibit development of *S. aureus* biofilms by preventing the activity of the *ica* genes, which are responsible for producing polysaccharide intercellular adhesins (PIA) [9,76,83]. These are the main extracellular polymeric components of 3D matrices encasing the bacterial cells during the biofilm formation [9,76,83]. In addition to the proposed antibacterial mechanisms of ω-3 PUFAs, it is important to note that the molecular shapes and structures of the major amphiphilic lipid constituents of coatings may

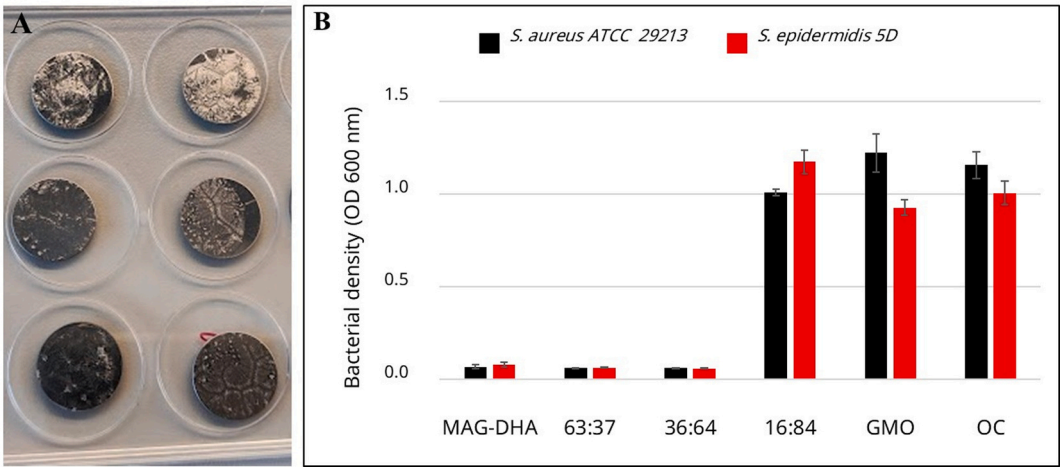

Fig. 4. (A) Representative SS discs coated with dry MAG-DHA and MAG-DHA/GMO binary lipid mixtures. (B) antibacterial activities of SS discs coated with MAG-DHA alone, and MAG-DHA/GMO binary lipid combinations (prepared at different MAG-DHA/GMO ratios of 63:37, 36:64, and 16:84) against *S. epidermidis* 5D and *S. aureus* ATCC 29213. After 24 h of incubation of the coated SS discs in bacterial cultures, the antibacterial activity was evaluated by measuring the bacterial density. The SS discs ($n = 3$) coated with dry lipid films of GMO alone, and overnight bacterial cultures (OC) of *S. aureus* ATCC 29213 and *S. epidermidis* 5D were used as controls.

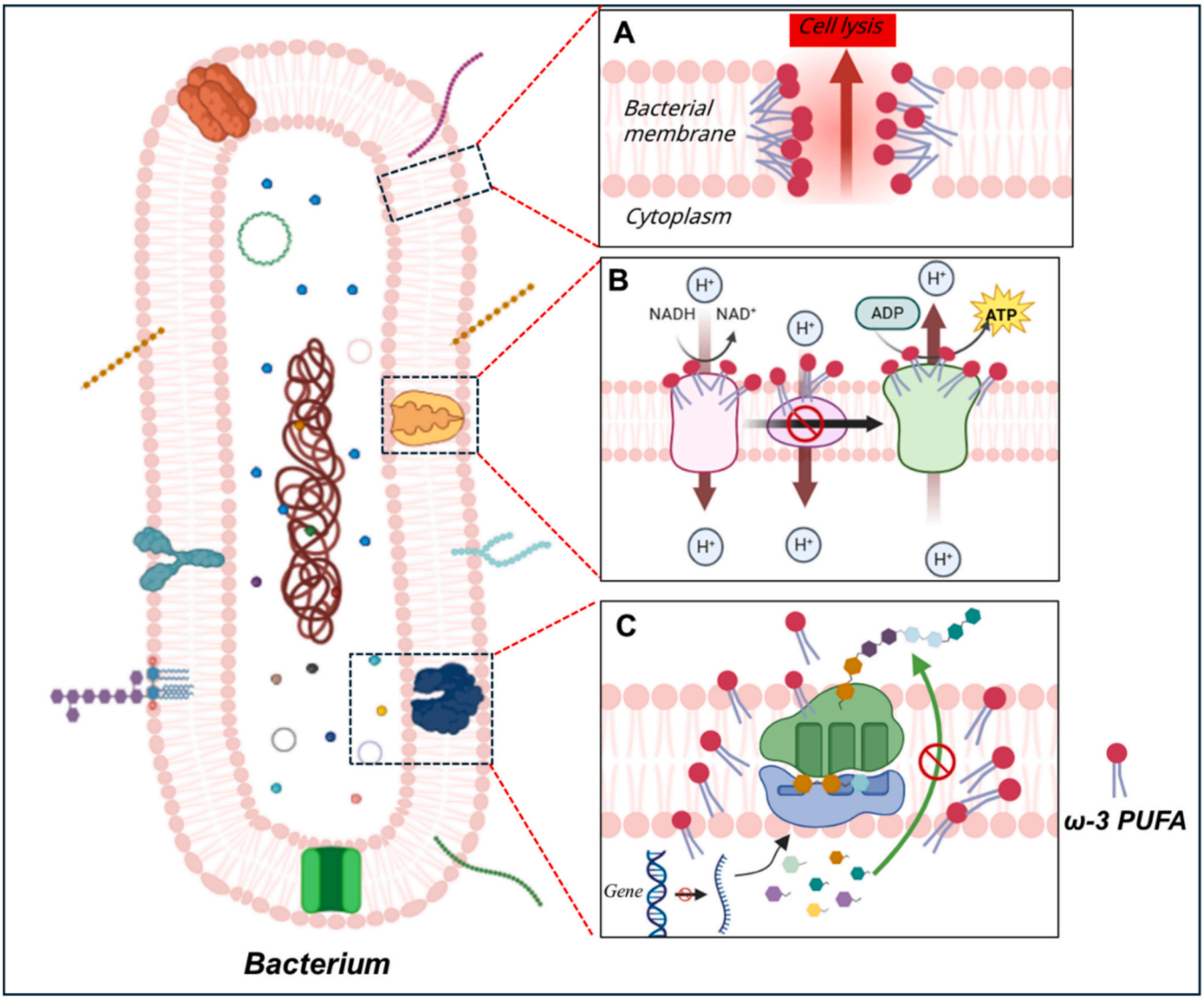

Fig. 5. Schematic representation of potential multiple antibacterial mechanisms of ω-3 PUFAs. A membrane-lytic behavior eventually leads to destabilization of the bacterial membranes through most likely the pore formation mechanism (A). The membrane-destabilizing activity by ω-3 PUFAs may also be attributed to a disruption of key biological processes such as the electron transport chain (B) and an inhibition of the production of membrane components such as polysaccharides (C). *Created with* biorender.com

play an important role in modulating the antibacterial efficacy against bacterial cell membranes. In line with recent studies [84], it is important for elucidating the antibiofilm nanostructure-activity relationship to consider that the inherent tendency of GMO and MAG-DHA to form highly curved inverted topologies (cubic *Pn3m* and H_2 phases) may enhance their bacterial cell membrane-disrupting capabilities. These amphiphiles most likely contribute to the molecular mechanisms of bacterial cell death through their tendency to induce significant alterations in the structural and permeability properties, and fluidity of the cell membranes and plausibly enhance solubilization of membrane proteins.

In this study, it was our interest to produce structurally tunable coatings with inherent antibiofilm activities and gain insight into the structure-activity relationship. In particular, we aimed at shedding light on the role of the structural features of inverse cubic and H_2 phases in modulating the antibiofilm efficacy. Based on our antibiofilm investigations (Fig. 4), there was no evidence that the cubic phase, owing to its relatively higher interfacial area and complex water channel networks, may facilitate a more effective presentation or release of MAG-DHA component as compared to the H_2 phase. The obtained results indicated that the local concentration of MAG-DHA plays a crucial role in enhancing the coating-bacterial membrane interactions and modulating therefore the antibiofilm activity. However, based on SAXS experiments at equilibrium and full hydration conditions and the out-of-equilibrium GISAXS analysis, MAG-DHA induced, in a concentration-dependent manner, phase transitions from inverse bicontinuous cubic phases to phases with more negative spontaneous curvatures (inverse discontinuous phases, including H_2 phases). For a more reliable assessment of the role of the structural features of inverse cubic and H_2 phases in modulating the antibiofilm efficacy, it is worth investigating the antibiofilm activities by using coatings built of these self-assemblies, which were produced at same concentration of MAG-DHA.

3.4. Time–kill assay for nanostructural coatings based on MAG-DHA alone and its combination with GMO

Time-kill investigations were conducted at 37 °C for 24 h of incubation of the coated SS discs in the bacteria suspensions. It was our

interest to assess the killing dynamics of the nanostructural coatings based on MAG-DHA alone, and its binary combinations with GMO (prepared at MAG-DHA/GMO ratios of 63:37, 36:64, and 16:84) against *S. aureus* ATCC 29213 and *S.epidermidis* 5D. In this study, the bacteria suspensions were used as controls. As shown in Fig. 6A, the results of the time-kill assays indicated no significant antibacterial effects against *S. aureus* ATCC 29213 for any of the investigated coatings within 1 h of incubation. After 2 h of exposure to the suspensions, a significant reduction in CFUs (decreasing from 4 $\log_{10}$ to 0 $\log_{10}$) was observed for coatings prepared using MAG-DHA alone or in combination with GMO at the highest MAG-DHA content (MAG-DHA/GMO ratio of 63:37). Further, the inherent antibacterial efficacies of these samples were sustained for 24 h, with no bacterial growth detected at the end of the experiments. At a lower MAG-DHA content (coatings prepared at MAG-DHA/GMO ratios of 36:64 and 16:84), the obtained results indicated a complete bacteria killing after 4 h of incubation, and the antibacterial effect was maintained at least for 6 h of post-incubation. However, bacterial regrowth started to evolve after 24 h of incubation of these two LLC coatings. It is still worth noting that the regrowth was more pronounced upon decreasing MAG-DHA content: an increase in the regrowth level from 4 $\log_{10}$ to a complete regrowth (9 $\log_{10}$) upon decreasing MAG-DHA/GMO ratio from 36:64 to 16:83, respectively (Fig. 6A).

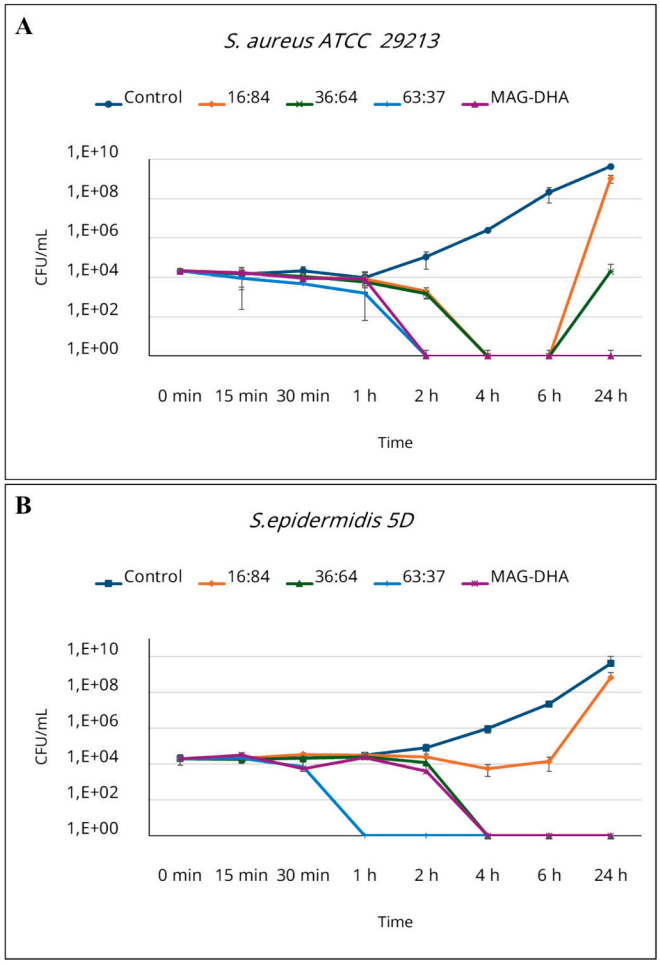

Fig. 6. Time-killing curves for nanostructural coatings based on MAG-DHA alone, and its binary mixtures with GMO (at the following three different lipid compositions (MAG-DHA/GMO ratios): 63:37, 36:64, and 16:84). The investigations were conducted against *S. aureus* ATCC 29213 (A) and *S. epidermidis* 5D (B). Each coating was tested in triplicate, and the data are presented as means of CFU/mL. Bacterial cultures alone (in absence of any test coatings) were used as controls.

In the study of the antibacterial activities of LLC coatings against *S. epidermidis* 5D, the ones with the lowest MAG-DHA/GMO ratio (16:84) exhibited only limited bacteriostatic effects for up to 6 h (4 $\log_{10}$, Fig. 6B). After this incubation time, no significant inhibition was detected, but instead an increase in the bacterial density was observed (Fig. 6B). In contrast, a complete bacterial killing was observed upon incubating LLC coatings containing a higher content of MAG-DHA. Augmenting MAG-DHA content was associated with a complete bacterial eradication within 1 h (at MAG-DHA/GMO ratio of 63:37), and 4 h (at MAG-DHA/GMO ratio of 36:64 and MAG-DHA alone). After 24 h of incubation, the antibacterial efficacies of LLC coatings based on MAG-DHA alone, and its two binary combinations with GMO (MAG-DHA/GMO ratios of 63:37 and 36:64) remained unchanged (0 $\log_{10}$).

At the lowest concentration of MAG-DHA (at a ratio of 16:84), the antibacterial activities of the LLC coatings against *S. aureus* and *S. epidermidis* were different. These coatings exhibited bactericidal (killing) effects against *S. aureus*, while showing bacteriostatic (inhibiting growth) effects against *S. epidermidis*. This is in line with recent studies on the role of the lipid composition of the cell membranes of Gram-positive bacteria in modulating the antibacterial activity of DHA [2,30]. As compared to *S. epidermidis* species, *S. aureus* cell membranes contain larger amounts of phospholipids, including phosphatidylglycerols (PGs) and lysyl-phosphatidylglycerols (lysyl-PGs), which are potential targets on exposure of the bacteria to DHA [2,30,85]. Regarding the observed bacterial regrowth on exposure of different LLC coatings containing relatively low MAG-DHA content (Fig. 6), it is most likely attributed to the use of DHA at concentrations lower than the required therapeutic doses (< 400 μg/mL). This may induce genetic alterations and tolerant phenotypes of the exposed bacteria, promoting their regrowth [2,10,29]. In the literature, it was reported on the tolerance and survival of *S. aureus* when exposed to growth-inhibiting bactericidal agents [86]. The regrowth observed at MAG-DHA/GMO ratios of 16:84 and 36:64 (Fig. 6A), seems to be caused by subpopulations of *S. aureus* that exhibit tolerance to MAG-DHA when exposed to concentrations below the required bactericidal concentrations. The tolerance mechanisms are subject to further investigations. Further, we do not exclude the possible presence of bacteria subpopulations that survived the initial bactericidal effect. Here, it is worth noting that the antibacterial characteristics of the investigated LLC coatings can be considered both time- and dose-dependent. This is in line with recent studies reporting on the dose-dependent antibacterial activity of DHA and EPA [8,30,87]. At relatively high MAG-DHA content, the bacteria killing effect is rapid (< 2 h against *S. aureus* and < 4 h against *S. epidermidis),* whereas a longer duration is needed for achieving a complete bacterial eradication, when using coatings containing relatively low concentrations of MAG-DHA.

Returning to our study, it is worth mentioning the importance of combining MAG-DHA with GMO for enhancing the durability of the coatings at the solid interfaces of SS discs. MAG-DHA tends to display an inverse micellar solution under limited hydration conditions, as was evident from the GISAXS findings (Fig. 3); whereas GMO forms a dry solid crystalline film. Thus, the observed difference in the antibacterial activity on exposure of MAG-DHA coatings to *S. aureus* and *S. epidermidis* (Fig. 6) can be attributed most likely to differences in the lipid compositions of the cell membranes of these species as mentioned above. Further, possible dynamic spreading of the micellar solution of MAG-DHA on the solid interface and its depletion in the initial incubation stage may contribute to the observed differences in the bacterial activity levels between MAG-DHA coatings and those based on the binary MAG-DHA/GMO mixtures at a relatively high content of MAG-DHA (MAG-DHA/GMO ratio of 63:37), particularly against *S. aureus* (Fig. 6).

4. Conclusion

LLC self-assemblies (including Q_2 and H_2 phases) are promising candidates in the development of safe and biocompatible antibacterial coatings owing to their unique and inherent structural features,

bioadhesive properties, and capability of sustaining the release of loaded cargos [31,88–90]. However, their utilization for production of antibacterial coatings for medical devices (including orthopedic implants) is rarely investigated. Here, considering the recent interest in designing biomimetic and flexible coatings for orthopedic implants, it was our interest to report on the structural characterization and antibacterial activities of a set of nanostructurally tunable coatings produced through a directed self-assembly of GMO (a well investigated lipid with non-lamellar liquid crystalline phase forming propensity) and MAG-DHA (a bioactive lipid with wide therapeutic potential), without the use of antibiotics. Further, the experimental findings may contribute to fundamental understanding of dynamic self-assembly of amphiphilic lipids on solid interfaces.

In this study, we focus through a simple-by-design approach on production of antibiotic-free self-assembled coatings, and their thorough structural characterization by using SAXS and *in situ* GISAXS investigations. Depending on lipid composition and RH level, the directed self-assembly of MAG-DHA and GMO on the solid interfaces led to generation of different self-assemblies (including swollen micelles and LLC self-assemblies (H_2 and Q_2 phases)). Further at relatively high concentration of MAG-DHA, the produced coatings showed strong inherent antibacterial activities against *S. aureus* and *S. epidermidis* bacteria, which are two of the most common orthopedic implant-related Gram-positive bacteria. These coatings are attractive for use to prevent bacteria attachment and subsequent biofilm formation on implants. They may find also applications in designing innovative multifunctional implant coatings for co-delivery of DHA and antibacterial agents in clinical settings, prior or during orthopedic surgeries.

In addition to their antibacterial properties, DHA and other ω-3 PUFAs are reported to have beneficial effects on bone health by protecting osteoblasts (bone-forming cells) from bacterial infections, promoting their differentiation and proliferation, and suppressing osteoclasts (bone-resorbing cells) [15,27,28]. Regarding the typical exposure of orthopedic implants to mechanical forces and frictions, the corrosion-inhibiting properties of these essential fatty acids present an additional advantage for their use in the design of implant coatings [5,91,92].

Processing and storage may affect the oxidative stability of the coatings. As MAG-DHA is highly prone to oxidation, it is important in future investigations to assess the stability of the coatings against oxidation in the presence and absence of antioxidants.

CRediT authorship contribution statement

Seref Akay: Writing – review & editing, Writing – original draft, Investigation, Funding acquisition, Formal analysis, Data curation, Conceptualization. **Oana Ciofu:** Writing – review & editing, Visualization, Validation, Supervision, Data curation, Conceptualization. **Jonathan Michael Gow:** Writing – review & editing, Validation, Investigation, Formal analysis. **Dorthe Posselt:** Writing – review & editing, Visualization, Validation, Supervision, Formal analysis, Data curation. **Benedetta Marmiroli:** Writing – review & editing, Validation, Methodology, Formal analysis, Data curation. **Barbara Sartori:** Writing – review & editing, Visualization, Validation, Methodology, Investigation, Formal analysis. **Anan Yaghmur:** Writing – review & editing, Writing – original draft, Validation, Supervision, Resources, Project administration, Formal analysis, Conceptualization.

Declaration of competing interest

The authors declare that they have no known competing financial interests or personal relationships that could have appeared to influence the work reported in this paper.

Acknowledgements

The study funded by the European Union's Horizon Europe under the Marie Skłodowska-Curie Postdoctoral Fellowships programme (Grant No: 101107704). The Novo Nordisk Foundation is gratefully acknowledged for funding RUCSAXS – Roskilde University Interdisciplinary X-ray Scattering Hub – with grant No: NNF21OC0068491. A.Y. further acknowledges financial support by the Danish Natural Sciences Research Council (DanScatt) for SAXS experiments and the Danish Council for Independent Research | Technology and Production Sciences (reference DFF-3105 00039B). S.A. acknowledge the CERIC-ERIC Consortium for access to the Austrian SAXS beamline at the Elettra Synchrotron (ELETTRA, Trieste, Italy).

Appendix A. Supplementary data

Supplementary data to this article can be found online at https://doi.org/10.1016/j.jcis.2025.139493.

Data availability

Data will be made available on request.

References

[1] K. Tang, J. Wang, X. Pei, Z. Zhu, J. Liu, Q. Wan, X. Zhang, Flexible coatings based on hydrogel to enhance the biointerface of biomedical implants, Adv. Colloid Interface Sci. 335 (2025) 103358, https://doi.org/10.1016/j.cis.2024.103358.
[2] D.C. Coraça-Huber, S. Steixner, A. Wurm, M. Nogler, Antibacterial and anti-biofilm activity of Omega-3 polyunsaturated fatty acids against Periprosthetic joint infections-isolated multi-drug resistant strains, Biomedicines 9 (2021) 334, https://doi.org/10.3390/biomedicines9040334.
[3] Y. Wang, B. Hong, B. Yin, Y. Li, L. Huang, S. Tan, T. Gao, M.F. Maitz, J. Zhang, S. Zheng, C. Huang, H. Qiu, J. Chen, X. Li, Engineering antibacterial, biocompatible, anti-oxidant titanium-based implants using polyphenols-chlorhexidine networks for bone regeneration, Adv. Healthc Mater 14 (2025) 2404958, https://doi.org/10.1002/adhm.202404958.
[4] M. Kariksiz, D. Kirkik, Antibacterial evaluation of antibiotic-coated titanium and stainless steel implants in orthopaedic application: a dip-coating approach, J. Orthop. Surg. Res. 20 (2025) 37, https://doi.org/10.1186/s13018-025-05467-y.
[5] I. Ul Haq, K. Krukiewicz, Antimicrobial approaches for medical implants coating to prevent implants associated infections: insights to develop durable antimicrobial implants, Appl. Surface Sci. Adv. 18 (2023) 100532, https://doi.org/10.1016/j.apsadv.2023.100532.
[6] C. Petzold, M. Gomez-Florit, S.P. Lyngstadaas, M. Monjo, EPA covalently bound to smooth titanium surfaces decreases viability and biofilm formation of *Staphylococcus epidermidis* in vitro, J. Orthop. Res. 30 (2012) 1384–1390, https://doi.org/10.1002/jor.22089.
[7] A. Udduttula, N. Jakubovics, I. Khan, L. Pontiroli, K.S. Rankin, P. Gentile, A. M. Ferreira, Layer-by-layer coatings of collagen–hyaluronic acid loaded with an antibacterial manuka honey bioactive compound to fight metallic implant infections, ACS Appl. Mater. Interfaces 15 (2023) 58119–58135, https://doi.org/10.1021/acsami.3c11910.
[8] Y.-G. Kim, J.-H. Lee, C.J. Raorane, S.T. Oh, J.G. Park, J. Lee, Herring oil and omega fatty acids inhibit *Staphylococcus aureus* biofilm formation and virulence, Front. Microbiol. 9 (2018) 365562, https://doi.org/10.3389/fmicb.2018.01241.
[9] C. Spiegel, S.J.M. Steixner, D.C. Coraça-Huber, Antibiofilm activity of Omega-3 fatty acids and its influence on the expression of biofilm formation genes on *Staphylococcus aureus*, Antibiotics 11 (2022) 932, https://doi.org/10.3390/antibiotics11070932.
[10] A.T. Zacher, K. Mirza, L. Thieme, S. Nietzsche, C. Senft, F. Schwarz, Biofilm formation of *Staphylococcus aureus* on various implants used for surgical treatment of destructive spondylodiscitis, Sci. Rep. 14 (2024) 19364, https://doi.org/10.1038/s41598-024-70244-6.
[11] F. Yang, J. Shi, Y. Wei, Q. Gao, J. Shen, L. Yin, H. Tang, Mixed-charge glycopolypeptides as antibacterial coatings with long-term activity, Chin. Chem. Lett. 36 (2025) 109746, https://doi.org/10.1016/j.cclet.2024.109746.
[12] P. Kumar, J.-H. Lee, H. Beyenal, J. Lee, Fatty acids as Antibiofilm and Antivirulence agents, Trends Microbiol. 28 (2020) 753–768, https://doi.org/10.1016/j.tim.2020.03.014.
[13] F. Liu, Y. Xue, Y. Zhou, J. Zhang, A. Wang, R. Shi, Trends and advances in antimicrobial surface modification for orthopedic implants (2014–2024), Tissue Eng. Part C Methods 31 (2025) 11–25, https://doi.org/10.1089/ten.tec.2024.0266.
[14] W. Liu, K. Zhang, Y. Sun, Z. Xiao, H. Hu, Z. Xiong, Y. Hu, Multidimensional treatment of periprosthetic joint infection using fusion peptide-grafted chitosan coated porous tantalum scaffold, Bioact. Mater 44 (2025) 15–33, https://doi.org/10.1016/j.bioactmat.2024.09.040.

[15] C. Spiegel, B. Ünalan, A. Kaserbacher, R. Arora, D.C. Coraça-Huber, Eicosapentaenoic acid and docosahexaenoic acid as an antimicrobial agent in orthopedics—an in vitro study about the race for surface, Pathogens 14 (2025) 57, https://doi.org/10.3390/pathogens14010057.
[16] M. Chen, W. Yu, Q. Shi, H. Wen, G. Li, Y. Wang, T. Wang, S. Liu, T. Yang, Boosting the anti-infection ability of titanium implants by coating polydopamine–curcumin, Coatings 14 (2024) 640, https://doi.org/10.3390/coatings14050640.
[17] L. Yang, L. Li, H. Li, T. Wang, X. Ren, Y. Cheng, Y. Li, Q. Huang, Layer-by-layer assembled smart antibacterial coatings via mussel-inspired polymerization and dynamic covalent chemistry, Adv. Healthc. Mater. 11 (2022) 2200112, https://doi.org/10.1002/adhm.202200112.
[18] T. Wei, Q. Yu, H. Chen, Responsive and synergistic antibacterial coatings: fighting against Bacteria in a smart and effective way, Adv. Healthc. Mater. 8 (2019) 1801381, https://doi.org/10.1002/adhm.201801381.
[19] D. Li, P. Lv, L. Fan, Y. Huang, F. Yang, X. Mei, D. Wu, The immobilization of antibiotic-loaded polymeric coatings on osteoarticular Ti implants for the prevention of bone infections, Biomater. Sci. 5 (2017) 2337–2346, https://doi.org/10.1039/C7BM00693D.
[20] S. Wu, J. Xu, L. Zou, S. Luo, R. Yao, B. Zheng, G. Liang, D. Wu, Y. Li, Long-lasting renewable antibacterial porous polymeric coatings enable titanium biomaterials to prevent and treat peri-implant infection, Nat. Commun. 12 (2021) 3303, https://doi.org/10.1038/s41467-021-23069-0.
[21] G. Gaetano, P. Giuseppe, P.F. Salvatore, M. Susanna, S. Sara, R.C. Luca, Hyaluronic-based antibacterial hydrogel coating for implantable biomaterials in orthopedics and trauma: from basic research to clinical applications, Hydrogels, InTech, 2018, https://doi.org/10.5772/intechopen.73203.
[22] M. Wang, Y. Zheng, C. Yin, S. Dai, X. Fan, Y. Jiang, X. Liu, J. Fang, B. Yi, Q. Zhou, T. Wang, Recent Progress in antibacterial hydrogel coatings for targeting biofilm to prevent orthopedic implant-associated infections, Front. Microbiol. 14 (2023) 1343202, https://doi.org/10.3389/fmicb.2023.1343202.
[23] V. Zarghami, M. Ghorbani, K.P. Bagheri, M.A. Shokrgozar, Improving bactericidal performance of implant composite coatings by synergism between Melittin and tetracycline, J. Mater. Sci. Mater. Med. 33 (2022) 46, https://doi.org/10.1007/s10856-022-06666-3.
[24] Y. Cheng, S. Mei, X. Kong, X. Liu, B. Gao, B. Chen, J. Wu, Long-term antibacterial activity of a composite coating on titanium for dental implant application, J. Biomater. Appl. 35 (2021) 643–654, https://doi.org/10.1177/0885328220963934.
[25] G.C. Cardoso, D.R.N. Correa, M. Fosca, E.V. Pometun, I.V. Antoniac, C.R. Grandini, J.V. Rau, Current strategies in developing antibacterial surfaces for joint arthroplasty implant applications, Materials 18 (2025) 173, https://doi.org/10.3390/ma18010173.
[26] Y. Li, H. Sung Min, C. Chen, H. Shan, Y. Lin, F. Yin, Y. Chen, L. Lu, X. Yu, A chitosan/gelatin/aldehyde hyaluronic acid hydrogel coating releasing calcium ions and vancomycin in pH response to prevent the formation of bacterial biofilm, Carbohydr. Polym. 347 (2025) 122723, https://doi.org/10.1016/j.carbpol.2024.122723.
[27] Z. Ali, M.A. Al-Ghouti, H. Abou-Saleh, M.M. Rahman, Unraveling the Omega-3 puzzle: navigating challenges and innovations for bone health and healthy aging, Mar. Drugs 22 (2024) 446, https://doi.org/10.3390/md22100446.
[28] A. Triantafyllou, P.P. Lelovas, A. Galanos, K. Venetsanou, C. Passali, A. Patsaki, D. Pitidis, S.K. Kourkoulis, I.A. Dontas, Fish oil consumption: its effects on bone and blood parameters of the Ovariectomized rat model of osteopenia, Nutrients 16 (2024) 4046, https://doi.org/10.3390/nu16234046.
[29] S. Park, J.-H. Lee, Y.-G. Kim, L. Hu, J. Lee, Fatty acids as aminoglycoside antibiotic adjuvants against *Staphylococcus aureus*, Front. Microbiol. 13 (2022) 876932, https://doi.org/10.3389/fmicb.2022.876932.
[30] H. Jan, S. Ghayas, D. Higazy, N.M. Ahmad, A. Yaghmur, O. Ciofu, Antibacterial and anti-biofilm activities of antibiotic-free phosphatidylglycerol/docosahexaenoic acid lamellar and non-lamellar liquid crystalline nanoparticles, J. Colloid Interface Sci. 669 (2024) 537–551, https://doi.org/10.1016/j.jcis.2024.04.186.
[31] Y. Chen, P. Ma, S. Gui, Cubic and hexagonal liquid crystals as drug delivery systems, Biomed. Res. Int. 2014 (2014) 1–12, https://doi.org/10.1155/2014/815981.
[32] A. Yaghmur, M. Rappolt, J. Østergaard, C. Larsen, S.W. Larsen, Characterization of bupivacaine-loaded formulations based on liquid crystalline phases and microemulsions: the effect of lipid composition, Langmuir 28 (2012) 2881–2889, https://doi.org/10.1021/la203577v.
[33] S. Akay, A. Yaghmur, Recent Advances in Antibacterial Coatings to Combat Orthopedic Implant-Associated Infections, Molecules 29 (2024) 1172, https://doi.org/10.3390/MOLECULES29051172.
[34] S. Akay, M. Nazim, R. Foroughian, C.K. Kristensen, D. Higazy, D. Posselt, O. Ciofu, A. Yaghmur, Liquid crystalline coatings loaded with colistin for preventing development of biofilms on orthopedic implants, J. Colloid Interface Sci. 687 (2025) 630–642, https://doi.org/10.1016/j.jcis.2025.02.107.
[35] X. Shao, G. Bor, S. Al-Hosayni, S. Salentinig, A. Yaghmur, Structural characterization of self-assemblies of new omega-3 lipids: docosahexaenoic acid and docosapentaenoic acid monoglycerides, Phys. Chem. Chem. Phys. 20 (2018) 23928–23941, https://doi.org/10.1039/C8CP04256J.
[36] A. Yaghmur, S. Al-Hosayni, H. Amenitsch, S. Salentinig, Structural investigation of bulk and dispersed inverse Lyotropic hexagonal liquid crystalline phases of Eicosapentaenoic acid Monoglyceride, Langmuir 33 (2017) 14045–14057, https://doi.org/10.1021/acs.langmuir.7b03078.
[37] R. Khaddaj-Mallat, C. Morin, É. Rousseau, Novel n-3 PUFA monoacylglycerides of pharmacological and medicinal interest: anti-inflammatory and anti-proliferative effects, Eur. J. Pharmacol. 792 (2016) 70–77, https://doi.org/10.1016/j.ejphar.2016.10.038.
[38] M.-F. Oye Mintsa Mi-mba, M. Lebbadi, W. Alata, C. Julien, V. Emond, C. Tremblay, S. Fortin, C.J. Barrow, J.-F. Bilodeau, F. Calon, Differential impact of eicosapentaenoic acid and docosahexaenoic acid in an animal model of Alzheimer's disease, J. Lipid Res. 65 (2024) 100682, https://doi.org/10.1016/j.jlr.2024.100682.
[39] C.M. Champigny, R.P.J. Cormier, C.J. Simard, P.-D. St-Coeur, S. Fortin, N. Pichaud, Omega-3 Monoacylglyceride effects on longevity, mitochondrial metabolism and oxidative stress: insights from drosophila melanogaster, Mar. Drugs 16 (2018) 453, https://doi.org/10.3390/md16110453.
[40] J.B. Hopkins, BioXTAS RAW 2: new developments for a free open-source program for small-angle scattering data reduction and analysis, J. Appl. Cryst. 57 (2024) 194–208, https://doi.org/10.1107/S1600576723011019.
[41] L. de Campo, A. Yaghmur, L. Sagalowicz, M.E. Leser, H. Watzke, O. Glatter, Reversible phase transitions in emulsified nanostructured lipid systems, Langmuir 20 (2004) 5254–5261, https://doi.org/10.1021/la0499416.
[42] G. Lindblom, L. Rilfors, Cubic phases and isotropic structures formed by membrane lipids — possible biological relevance, Biochimica et Biophysica Acta (BBA) - Rev. Biomembranes 988 (1989) 221–256, https://doi.org/10.1016/0304-4157(89)90020-8.
[43] R.V.M. Freire, B. Tran, M. Debas, M. Zabara, H. Amenitsch, S. Salentinig, Nanostructure formation in Glycerolipid films during enzymatic hydrolysis: a GISAXS study, ACS Appl. Mater. Interfaces 16 (2024) 61262–61271, https://doi.org/10.1021/acsami.4c12125.
[44] D.-M. Smilgies, Grazing-Incidence Small-Angle Scattering (GISAXS), in: The SAXS Guide, 4th ed, Anton Paar, Graz, 2017, pp. 109–123.
[45] Y. Ezoe, T. Shirata, T. Ohashi, M. Ishida, K. Mitsuda, K. Fujiwara, K. Morishita, K. Nakajima, Development of high-resolution and light-weight x-ray optics with deformed silicon wafers, in: R. Hudec, L. Pina (Eds.), EUV and X-Ray Optics: Synergy between Laboratory and Space, SPIE, Prag, 2009 73600B, https://doi.org/10.1117/12.823932.
[46] G. Renaud, R. Lazzari, F. Leroy, Probing surface and interface morphology with grazing incidence small angle X-ray scattering, Surf. Sci. Rep. 64 (2009) 255–380, https://doi.org/10.1016/j.surfrep.2009.07.002.
[47] A. Hexemer, P. Müller-Buschbaum, Advanced grazing-incidence techniques for modern soft-matter materials analysis, IUCrJ 2 (2015) 106–125, https://doi.org/10.1107/S2052252514024178.
[48] B. Marmiroli, B. Sartori, A.R. Kyvik, I. Ratera, H. Amenitsch, Structural study of the hydration of lipid membranes upon interaction with mesoporous supports prepared by standard methods and/or X-ray irradiation, Front Mater 8 (2021), https://doi.org/10.3389/fmats.2021.686353.
[49] M. Rappolt, Bilayer thickness estimations with "poor" diffraction data, J. Appl. Phys. 107 (2010), https://doi.org/10.1063/1.3393600.
[50] H. Amenitsch, M. Rappolt, C.V. Teixeira, M. Majerowicz, P. Laggner, In situ sensing of salinity in oriented lipid multilayers by surface X-ray scattering, Langmuir 20 (2004) 4621–4628, https://doi.org/10.1021/la036319p.
[51] H. Amenitsch, M. Rappolt, M. Kriechbaum, H. Mio, P. Laggner, S. Bernstorff, First performance assessment of the small-angle X-ray scattering beamline at ELETTRA, J. Synchrotron Radiat. 5 (1998) 506–508, https://doi.org/10.1107/S090904959800137X.
[52] P. Sharifi, B. Marmiroli, B. Sartori, F. Cacho-Nerin, J. Keckes, H. Amenitsch, O. Paris, Humidity-driven deformation of ordered mesoporous silica films, bioinspired, Biomimetic Nanobiomaterials 3 (2014) 183–190, https://doi.org/10.1680/bbn.14.00017.
[53] M. Burian, C. Meisenbichler, D. Naumenko, H. Amenitsch, *SAXSDOG* : open software for real-time azimuthal integration of 2D scattering images, J. Appl. Cryst. 55 (2022) 677–685, https://doi.org/10.1107/S1600576722003685.
[54] M. Rittman, H. Amenitsch, M. Rappolt, B. Sartori, B.M.D. O'Driscoll, A.M. Squires, Control and analysis of oriented thin films of lipid inverse Bicontinuous cubic phases using grazing incidence small-angle X-ray scattering, Langmuir 29 (2013) 9874–9880, https://doi.org/10.1021/la401580y.
[55] G.D. Kalaycioglu, G. Bor, A. Yaghmur, Simple-by-design approach for production of stabilizer-free cubosomes from phosphatidylglycerol and docosahexaenoic acid monoacylglycerol, J. Colloid Interface Sci. 675 (2024) 825–835, https://doi.org/10.1016/j.jcis.2024.07.077.
[56] J. Clogston, J. Rathman, D. Tomasko, H. Walker, M. Caffrey, Phase behavior of a monoacylglycerol, Chem. Phys. Lipids 107 (2000) 191–220, https://doi.org/10.1016/S0009-3084(00)00182-1.
[57] B. Angelov, A. Angelova, U. Vainio, V.M. Garamus, S. Lesieur, R. Willumeit, P. Couvreur, Long-living intermediates during a lamellar to a diamond-cubic lipid phase transition: a small-angle X-ray scattering investigation, Langmuir 25 (2009) 3734–3742, https://doi.org/10.1021/la804225j.
[58] P. Wadsten-Hindrichsen, J. Bender, J. Unga, S. Engström, Aqueous self-assembly of phytantriol in ternary systems: effect of monoolein, distearoylphosphatidylglycerol and three water-miscible solvents, J. Colloid Interface Sci. 315 (2007) 701–713, https://doi.org/10.1016/j.jcis.2007.07.011.
[59] T. Kamo, M. Nakano, W. Leesajakul, A. Sugita, H. Matsuoka, T. Handa, Nonlamellar liquid crystalline phases and their particle formation in the egg yolk phosphatidylcholine/Diolein system, Langmuir 19 (2003) 9191–9195, https://doi.org/10.1021/la035313x.
[60] A. Yaghmur, L. de Campo, L. Sagalowicz, M.E. Leser, O. Glatter, Control of the internal structure of MLO-based Isasomes by the addition of Diglycerol Monooleate and soybean phosphatidylcholine, Langmuir 22 (2006) 9919–9927, https://doi.org/10.1021/la061303v.

[61] D. Smilgies, <scp>GISAXS</scp> : a versatile tool to assess structure and self-assembly kinetics in block copolymer thin films, J. Polym. Sci. 60 (2022) 1023–1041, https://doi.org/10.1002/pol.20210244.
[62] P. Müller-Buschbaum, Grazing incidence small-angle X-ray scattering: an advanced scattering technique for the investigation of nanostructured polymer films, Anal. Bioanal. Chem. 376 (2003) 3–10, https://doi.org/10.1007/s00216-003-1869-2.
[63] M. Zabara, Q. Ren, H. Amenitsch, S. Salentinig, Bioinspired antimicrobial coatings from peptide-functionalized liquid crystalline nanostructures, ACS Appl. Bio Mater. 4 (2021) 5295–5303, https://doi.org/10.1021/acsabm.1c00415.
[64] S. Salentinig, M. Zabara, P. Parisse, H. Amenitsch, Formation of highly ordered liquid crystalline coatings – an *in situ* GISAXS study, Phys. Chem. Chem. Phys. 20 (2018) 21903–21909, https://doi.org/10.1039/C8CP03205J.
[65] S.J. Richardson, P.A. Staniec, G.E. Newby, J.L. Rawle, A.R. Slaughter, N.J. Terrill, J.M. Elliott, A.M. Squires, Glycerol prevents dehydration in lipid cubic phases, Chem. Commun. 51 (2015) 11386–11389, https://doi.org/10.1039/C5CC03771A.
[66] S. Björklund, V. Kocherbitov, Hydration-induced phase transitions in surfactant and lipid films, Langmuir 32 (2016) 5223–5232, https://doi.org/10.1021/acs.langmuir.6b00452.
[67] M. Morin, S. Björklund, E.J. Nilsson, J. Engblom, Bicontinuous cubic liquid crystals as potential matrices for non-invasive topical sampling of low-molecular-weight biomarkers, Pharmaceutics 15 (2023) 2031, https://doi.org/10.3390/pharmaceutics15082031.
[68] J.J. van Franeker, D. Hermida-Merino, C. Gommes, K. Arapov, J.J. Michels, R.A. J. Janssen, G. Portale, Sub-micrometer structure formation during spin coating revealed by time-resolved in situ laser and X-ray scattering, Adv. Funct. Mater. 27 (2017) 1702516, https://doi.org/10.1002/adfm.201702516.
[69] H. Okuda, M. Kato, K. Kuno, S. Ochiai, N. Usami, K. Nakajima, O. Sakata, A grazing incidence small-angle x-ray scattering analysis on capped Ge nanodots in layer structures, J. Phys. Condens. Matter 22 (2010) 474003, https://doi.org/10.1088/0953-8984/22/47/474003.
[70] T. Vu, N. Mahadevapuram, G.M. Perera, G.E. Stein, Controlling domain orientations in thin films of AB and ABA block copolymers, Macromolecules 44 (2011) 6121–6127, https://doi.org/10.1021/ma2009222.
[71] J. Jackman, B. Yoon, D. Li, N.-J. Cho, Nanotechnology formulations for antibacterial free fatty acids and Monoglycerides, Molecules 21 (2016) 305, https://doi.org/10.3390/molecules21030305.
[72] C.P. Churchward, R.G. Alany, L.A.S. Snyder, Alternative antimicrobials: the properties of fatty acids and monoglycerides, Crit. Rev. Microbiol. 44 (2018) 561–570, https://doi.org/10.1080/1040841X.2018.1467875.
[73] W. Wang, R. Wang, G. Zhang, F. Chen, B. Xu, In vitro antibacterial activities and mechanisms of action of fatty acid Monoglycerides against four foodborne Bacteria, J. Food Prot. 83 (2020) 331–337, https://doi.org/10.4315/0362-028X.JFP-19-259.
[74] Š. Petra, K. Věra, H. Iva, H. Petr, K. Zdeňka, B. Leona, Formulation, antibacterial activity, and cytotoxicity of 1-monoacylglycerol microemulsions, Eur. J. Lipid Sci. Technol. 116 (2014) 448–457, https://doi.org/10.1002/ejlt.201300171.
[75] C.Q. Sun, C.J. O'Connor, A.M. Roberton, Antibacterial actions of fatty acids and monoglycerides against *Helicobacter pylori*, FEMS Immunol. Med. Microbiol. 36 (2003) 9–17, https://doi.org/10.1016/S0928-8244(03)00008-7.
[76] Y. Lu, W. Cai, Z. Ren, P. Han, The role of staphylococcal biofilm on the surface of implants in orthopedic infection, Microorganisms 10 (2022) 1909, https://doi.org/10.3390/microorganisms10101909.
[77] C. Morin, R. Hiram, E. Rousseau, P.U. Blier, S. Fortin, Docosapentaenoic acid monoacylglyceride reduces inflammation and vascular remodeling in experimental pulmonary hypertension, Am. J. Physiology-Heart Circulatory Physiol. 307 (2014) H574–H586, https://doi.org/10.1152/ajpheart.00814.2013.
[78] C. Morin, P.U. Blier, S. Fortin, Eicosapentaenoic acid and docosapentaenoic acid monoglycerides are more potent than docosahexaenoic acid monoglyceride to resolve inflammation in a rheumatoid arthritis model, Arthritis Res. Ther. 17 (2015) 142, https://doi.org/10.1186/s13075-015-0653-y.
[79] C. Cruz-Hernandez, F. Destaillats, S.K. Thakkar, L. Goulet, E. Wynn, D. Grathwohl, C. Roessle, S. de Giorgi, L. Tappy, F. Giuffrida, V. Giusti, Monoacylglycerol-enriched oil increases EPA/DHA delivery to circulatory system in humans with induced lipid malabsorption conditions, J. Lipid Res. 57 (2016) 2208–2216, https://doi.org/10.1194/jlr.P070144.
[80] B. Cuenoud, I. Rochat, M. Gosoniu, L. Dupuis, E. Berk, A. Jaudszus, J. Mainz, G. Hafen, M. Beaumont, C. Cruz-Hernandez, Monoacylglycerol form of omega-3s improves its bioavailability in humans compared to other forms, Nutrients 12 (2020) 1014, https://doi.org/10.3390/nu12041014.
[81] G. Casillas-Vargas, C. Ocasio-Malavé, S. Medina, C. Morales-Guzmán, R.G. Del Valle, N.M. Carballeira, D.J. Sanabria-Ríos, Antibacterial fatty acids: an update of possible mechanisms of action and implications in the development of the next-generation of antibacterial agents, Prog. Lipid Res. 82 (2021) 101093, https://doi.org/10.1016/j.plipres.2021.101093.
[82] B. Yoon, J. Jackman, E. Valle-González, N.-J. Cho, Antibacterial free fatty acids and Monoglycerides: biological activities, experimental testing, and therapeutic applications, Int. J. Mol. Sci. 19 (2018) 1114, https://doi.org/10.3390/ijms19041114.
[83] C. Formosa-Dague, C. Feuillie, A. Beaussart, S. Derclaye, S. Kucharíková, I. Lasa, P. Van Dijck, Y.F. Dufrêne, Sticky matrix: adhesion mechanism of the staphylococcal polysaccharide intercellular Adhesin, ACS Nano 10 (2016) 3443–3452, https://doi.org/10.1021/acsnano.5b07515.
[84] J. Jennings, D. Ašćerić, E.F. Semeraro, K. Lohner, N. Malanovic, G. Pabst, Combinatorial screening of cationic Lipidoids reveals how molecular conformation affects membrane-targeting antimicrobial activity, ACS Appl. Mater. Interfaces 15 (2023) 40178–40190, https://doi.org/10.1021/ACSAMI.3C05481.
[85] G.C. Monnot, M. Wegrecki, T.-Y. Cheng, Y.-L. Chen, B.N. Sallee, R. Chakravarthy, I. M. Karantza, S.Y. Tin, A.E. Khaleel, I. Monga, L.N. Uwakwe, A. Tillman, B. Cheng, S. Youssef, S.W. Ng, A. Shahine, J.A. Garcia-Vilas, A.-C. Uhlemann, L.A. Bordone, A. Han, C.H. Rohde, G. Ogg, D.B. Moody, J. Rossjohn, A. de Jong, Staphylococcal phosphatidylglycerol antigens activate human T cells via CD1a, Nat. Immunol. 24 (2023) 110–122, https://doi.org/10.1038/s41590-022-01375-z.
[86] E.V.K. Ledger, A.M. Edwards, Growth arrest of *Staphylococcus aureus* induces daptomycin tolerance via cell wall remodelling, mBio 14 (1) (Feb. 2023), https://doi.org/10.1128/mbio.03558-22.
[87] N.R. Devi, S. Khandelwal, M. Subramaniyan, S. Pappu, Extraction, characterization, and therapeutic potential of Omega-3 fatty acids from *Belone belone* skin, 3 Biotech 14 (2024) 42, https://doi.org/10.1007/s13205-023-03885-5.
[88] A. Yaghmur, S. Ghayas, H. Jan, G.D. Kalaycioglu, S.M. Moghimi, Omega-3 fatty acid nanocarriers: characterization and potential applications, Curr. Opin. Colloid Interface Sci. 67 (2023) 101728, https://doi.org/10.1016/j.cocis.2023.101728.
[89] J. De Souza, K. Pontes, T. Alves, V. Amaral, M. Rebelo, M. Hausen, M. Chaud, Spotlight on biomimetic systems based on Lyotropic liquid crystal, Molecules 22 (2017) 419, https://doi.org/10.3390/molecules22030419.
[90] J.S.L. Leu, J.J.X. Teoh, A.L.Q. Ling, J. Chong, Y.S. Loo, I.D. Mat Azmi, N.I. Zahid, R. J.C. Bose, T. Madheswaran, Recent advances in the development of liquid crystalline nanoparticles as drug delivery systems, Pharmaceutics 15 (2023) 1421, https://doi.org/10.3390/pharmaceutics15051421.
[91] A. Dehghani, B. Ramezanzadeh, M. Mahdavian, Current Applications of Fatty Acids, Lignin, and Lipids as Green Corrosion Inhibitors, Handbook of Biomolecules, Elsevier, 2023, pp. 535–550, https://doi.org/10.1016/B978-0-323-91684-4.00030-X.
[92] A. Khanra, M. Srivastava, M.P. Rai, R. Prakash, Application of unsaturated fatty acid molecules derived from microalgae toward mild steel corrosion inhibition in hcl solution: a novel approach for metal–inhibitor association, ACS Omega 3 (2018) 12369–12382, https://doi.org/10.1021/acsomega.8b01089.